Effect of Boundary Layer Swirl on Supersonic Jet Instabilities and Thrust

SangYeop Han*

Senior Researcher, Rocket Engine Research Department, Propulsion System Research & Development Division, Korea Aerospace Research Institute

This paper reports the effects of nozzle exit boundary layer swirl on the instability modes of underexpanded supersonic jets emerging from plane rectangular nozzles. The effects of boundary layer swirl at the nozzle exit on thrust and mixing of supersonic rectangular jets are also considered. The previous study was performed with a 30° boundary layer swirl (S=0.41) in a plane rectangular nozzle exit. At this study, a 45° boundary layer swirl (S=1.0) is applied in a plane rectangular nozzle exit. A three-dimensional unsteady compressible Reynolds-Averaged Navier-Stokes code with Baldwin-Lomax and Chien's k-ε two-equation turbulence models was used for numerical simulation. A shock adaptive grid system was applied to enhance shock resolution. The nozzle aspect ratio used in this study was 5.0, and the fully-expanded jet Mach number was 1.526. The "*flapping*" and "*pumping*" oscillations were observed in the jet's small dimension at frequencies of about 3,900Hz and 7,800Hz, respectively. In the jet's large dimension, "*spanwise*" oscillations at the same frequency as the small dimension's "*flapping*" oscillations were captured. As reported before with a 30° nozzle exit boundary layer swirl, the induction of 45° swirl to the nozzle exit boundary layer also strongly enhances jet mixing with the reduction of thrust by 10%.

Key Words: Swirl, Instability, Flapping Oscillations, Pumping Oscillations, Spanwise Oscillations, Supersonic Jet

Nomenclature

AR : Nozzle aspect ratio, w/h
G : Velocity vector ratio
h : Nozzle exit small dimension, mm
M : Mach number
P : Pressure, N/m^2
p : Non-dimensionalized pressure
S : Degree of swirl
w : Nozzle exit large dimension, mm
u, v, w : Non-dimensionalized velocities in ξ, η, ζ-directions
x, y, z : Cartesian physical coordinates
θ : Swirl angle, degree

Subscript

atm : Atmospheric
j : Jet
max : Maximum
s : Static

* **E-mail** : syhan@kari.re.kr
TEL : +82-42-860-2051; **FAX** : +82-42-860-2602
Senior Researcher, Rocket Engine Research Department, Propulsion System Research & Development Division, Korea Aerospace Research Institute, 52 Oun-dong, Yusong-ku, Daejeon 305-333, Korea.(Manuscript **Received** July 6, 2000; **Revised** February 27, 2001)

1. Introduction

Turbulent mixing is largely responsible for generating jet noise. Broadband shock-associated noise and screech are also generated when a nozzle operates at off-design conditions. The characteristics of both mixing and shock-associated noise can be predicted by examining the jet flowfield (Kim *et al.*, 1994).

Prediction of supersonic jet noise requires an ability to accurately simulate the mean flow

structure and the interaction of jet's under/overexpansion shocks with the turbulent mixing layer. To compute a generalized supersonic jet flowfield with subsonic external streams, a three-dimensional computational code, which solves the Reynolds-Averaged Navier-Stokes equations in a time-asymptotic manner with suitable turbulence models is required. Computational simulations of underexpanded supersonic rectangular jets using Reynolds-Averaged Navier-Stokes equations were performed by Dash *et al.* (1990), Kim *et al.* (1994), and Han and Taghavi (1998) using various turbulence models (e.g. Chien's k-ϵ two-equation model and improved turbulence models for compressibility, energy-balance, and length-scale).

Under imperfectly expanded conditions, Kim *et al.* (1994) stated that the existence of shock cell structure and its interaction with the convecting turbulence structure may not only generate a broadband shock-associated noise but also change the turbulence structure, and thus the strength of mixing noise source.

From Han and Taghavi (1998), the frequency of flapping oscillations in the jet's small dimension, which were observed in an underexpanded supersonic rectangular jet at a fully-expanded Mach number of 1.526 with $AR=5.0$, was found to be about 7,500Hz. This result agreed with Raman's (1996) experimental value of 7,400Hz. Also, they found that the frequency of pumping oscillations in the jet's large dimension was twice as high as the flapping frequency, which was observed in the experiments of Suda *et al.* (1993). They used a high aspect ratio plane rectangular nozzle to simulate two-dimensional jets. Two modes of jet oscillations, flapping and symmetrical modes, were observed in their results. They also found dynamic behavior and a traveling wave inside the third shock cell in the flapping mode, and the traveling wave was the dominant source of screech sound generation.

Current study deals with swirling flows which are important in the design of various devices such as combustion chambers, spray nozzles, environmental units, etc. In the area of combustion, swirl addition to primary air and injected fuel is used to aid in flame stabilization and efficiency augmentation of high intensity combustion process in applications such as gasoline and diesel engines, liquid rocket engines, gas turbines, industrial furnaces, utility boilers, and many others (Gupta *et al.*, 1984; Kim *et al.*, 2000). Previous experimental studies indicated that swirl had large-scale effects on the jet flowfield (e.g. jet growth, mixing, flame size, shape, stability, and combustion intensity).

Mode switching phenomena of supersonic jets with swirl were studied experimentally by Yu *et al.* (1998). The fully-expanded Mach numbers up to 1.8 were studied. They observed the effects of swirl on flow recirculation, screech tone frequency, and phase information. Their results showed the existence of a quasi-periodic shock structure in strongly swirling jets in spite of swirl-generated recirculation; and helical and toroidal screech tones in strongly swirling jets. Also, they found that the swirl could induce flow recirculation in the first and second shock cell regions of supersonic jets.

To find the effect of nozzle exit boundary layer swirl on the instability modes of the underexpanded supersonic rectangular jet, Han and Taghavi (1999) simulated an underexpanded supersonic rectangular jet with a fully-expanded Mach number of 1.526, an aspect ratio of 5.0, and a 30° nozzle exit boundary layer swirl ($S=0.41$). Here, the swirl number S is defined as

$$S=\frac{G}{G-2},\ G=\frac{w_{\max}}{u_{\max}}$$

Their investigation showed flapping oscillations with a frequency of about 15,000Hz in the jet's small dimension and pumping oscillations in the jet's large dimension with a frequency twice as high as the flapping frequency. In the jet's large dimension, a new instability mode of spanwise oscillations, which had the same frequency as the flapping oscillations in the jet's small dimension, was found.

The primary purpose of this study is to further investigate the effect of nozzle exit boundary layer swirl on the instability modes of an under-

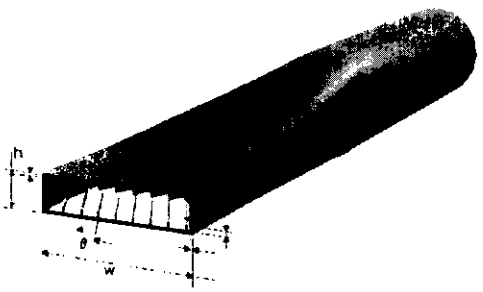

Fig. 1 Plane rectangular nozzle with nozzle exit boundary layer swirl vanes: h=6.0mm, w=30.0mm, θ=45°

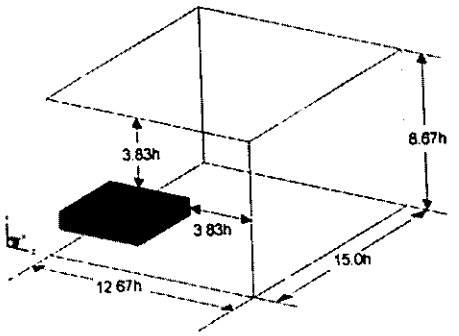

Fig. 2 Computational domain. Grid: 61×53×77

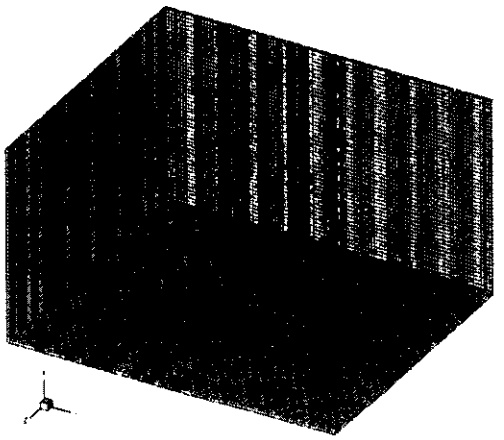

Fig. 3 Shock adaptive grid system. Grid: 148×53×77

expanded supersonic rectangular jet. In addition, thrust penalty due to the boundary layer swirlat the nozzle exit is also studied. At this stage, the underexpanded supersonic jet emerging from a plane rectangular nozzle of AR=5.0 at the fully-expanded Mach number of 1.526 with a 45° nozzle exit boundary layer swirl (S=1.0) is considered.

2. Computation

2.1 Code

To computationally simulate an underexpanded supersonic rectangular jet, a three-dimensional, unsteady, compressible, Reynolds-Averaged Navier-Stokes code is used with a shock-adaptive grid generator developed by the author. Baldwin-Lomax and Chien's k-ε two-equation turbulence models are used.

The code uses the three-dimensional compressible full Navier-Stokes equations in strong conservation form, using vector notation in the Cartesian coordinates, as the governing equations. The governing equations are solved by using the generalized scheme of Beam and Warming temporally and second-order central difference scheme spatially. To treat spatial derivatives at the boundaries, Neumann boundary conditions are applied using a first- or second-order one-sided difference scheme.

In addition, artificial viscosity is added to suppress high frequency instabilities which occur when shock waves are captured by a finite difference algorithm. In high Reynolds number flows, the odd-even decoupling produces those high frequency instability oscillations from the use of a second-order central difference scheme for the inviscid flux terms. To treat those instabilities, both explicit and implicit artificial viscosity models of Steger (1978) and an explicit nonlinear coefficient model (Jameson *et al.*, 1981) are applied. The fourth-order differences for explicit smoothing and the second-order differences for implicit smoothing are used.

With the above numerical technique, turbulence models are treated in the following manner. First, the initial calculation, using Baldwin-Lomax turbulence model, is carried out until reasonable residuals of primitive variables are achieved. Second, an intermediate flowfield is simulated with Chien's k-ε two-equation turbulence model using the results from the initial calculation. Last, the final simulation, using the

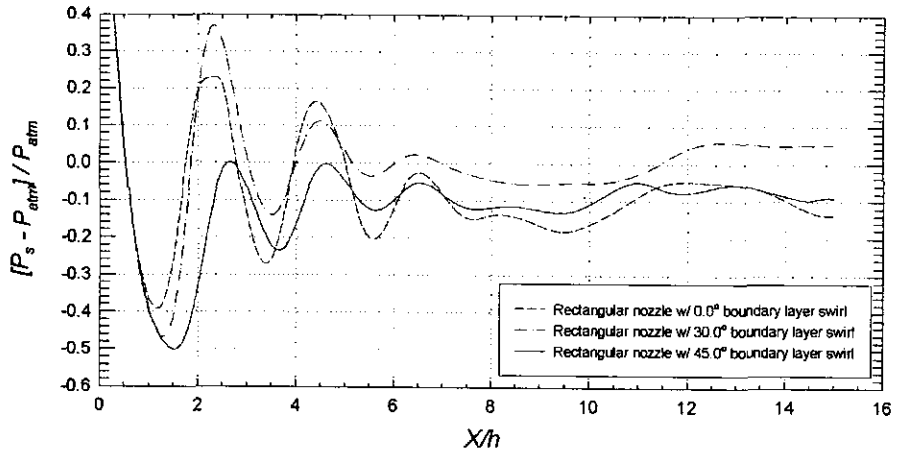

Fig. 4 Nozzle exit boundary layer swirl angle effects on nozzle centerline static pressure: M_j=1.526

intermediate results as the initial condition, is executed with a shock adaptive grid as explained later in Sec. 2.2.

2.2 Nozzle configuration and grid system

Placing a series of swirling vanes in the boundary layer at the nozzle exit could be an effective method for passive excitation in supersonic jets (Frank, 1994; Han and Taghavi, 1999). The nozzle configuration used in this study has been investigated as an effective tool for mixing enhancement of supersonic jets.

The convergent nozzle used in this study has a plane rectangular shape exit as shown in Fig. 1. The swirl is induced at 45° in the counter-clockwise direction to the nozzle exit boundary layer. The nozzle has an aspect ratio of 5.0. Experimental studies using the nozzle without nozzle exit boundary layer swirl have already been carried out by other researchers (Frank, 1994; Raman, 1996; Han and Taghavi, 1998; Raman and Taghavi, 1998; Kim and Lee, 2000).

Due to the three-dimensional nature of flow, a full three-dimensional computational domain as shown in Fig. 2 is used with a shock adaptive grid system shown in Fig. 3. The shock adaptive grid shows three shock cell locations. The initial computation is executed with a uniform $61\times53\times77$ structured grid system. After the initial computation, a shock adaptive grid generator is applied to the results to locate shocks and generate a grid system with 20% packing rate at the nozzle centerline shock locations as shown in Fig. 3. The shock adaptive grid system has the grid size of $148\times53\times77$.

2.3 Boundary conditions

Base boundary conditions are selected such that the boundaries outside nozzle exit and nozzle wall have zero gradients for pressure and velocities (Han and Taghavi, 1998). At the nozzle exit, the flow is choked and the exit pressure has the value of p=2.014, which corresponds to a fully-expanded Mach number of 1.526. At the nozzle exit plane, the flow outside the boundary layer has velocity condition with $u=1.0$ and $v=w=0.0$. Inside the exit boundary layer, the θ=45° swirl condition is set with the following configuration and velocities:

Swirl vanes are installed in a series manner inside a nozzle exit boundary layer with a vane angle of 45°, as shown in Fig. 1. Grid points where the boundary layer swirl is introduced have the following velocity boundary conditions:

Top :	$u=1.0$,	$v=0.0$,	$w=\sin 45°$
Bottom:	$u=1.0$,	$v=0.0$,	$w=-\sin 45°$
Right:	$u=1.0$,	$v=\sin 45°$,	$w=0.0$
Left:	$u=1.0$,	$v=-\sin 45°$,	$w=0.0$

3. Results and Discussion

In this section, the computational results of 45°

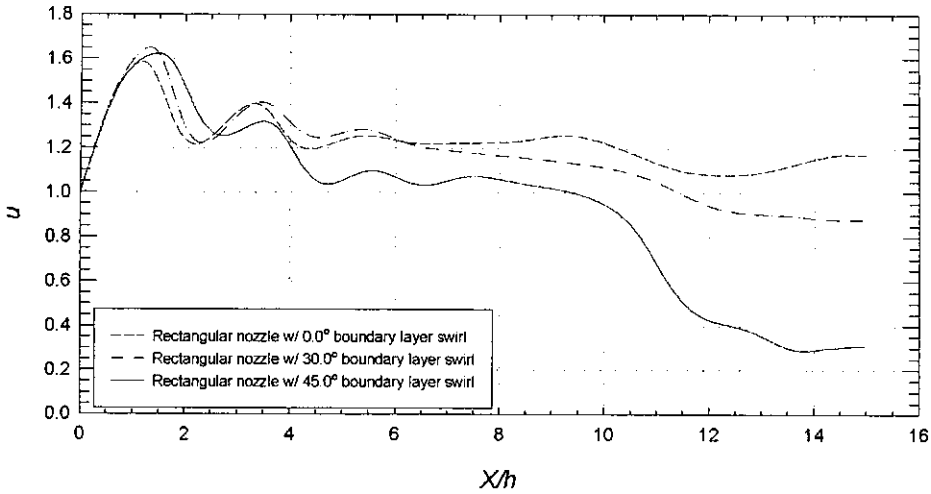

Fig. 5 Nozzle exit boundary layer swirl angle effects on nozzle centerline axial velocity: M_j=1.526

nozzle exit boundary layer swirl are described and compared with 0° and 30° nozzle exit boundary layer swirl cases.

Figure 4 has the collection of nozzle centerline static pressure distributions in the axial direction for the plane rectangular nozzle with 0°, 30°, and 45° nozzle exit boundary layer swirl (S=0.0, 0.41, 1.0 respectively). The data in Fig. 4 are chosen at a phase, which shows the maximum strength of the first shock cell. In all three cases two major shock cells and one relatively weak shock cell at the nozzle centerline are observed. In the first shock cell, the shock strength for 45° nozzle exit boundary layer swirl case is 20% less than the 0° swirl case and 41% less than the 30° swirl case. For the second shock cell, the shock strength for a 45° nozzle exit boundary layer swirl case is 46% less than the 0° swirl case and 9% less than the 30° swirl case. The third shock cell in the 45° nozzle exit boundary layer swirl is 57% weaker than the 0° swirl case and 27% stronger than the 30° swirl case. With three cases of nozzle exit boundary layer swirl angles a consistent relation between shock strength and nozzle exit boundary layer swirl angle is not found. However, the shock strength in the second shock cell of an underexpanded supersonic jet emerging from the plane rectangular nozzle becomes weaker as the angle of nozzle exit boundary layer swirl increases. Thus, nozzle exit boundary layer swirl angle affects the flowfield of underexpanded supersonic rectangular jet.

Nozzle centerline axial velocity distributions in the axial direction for all three cases are shown in Fig. 5. The data in Fig. 5 are taken at the same phase as those in Fig. 4. The jet velocity decay starts earlier as the nozzle exit boundary layer swirl angle increases. Also, the jet velocity decay is faster as the nozzle exit boundary layer swirl angle increases, and this trend suggests that mixing is enhanced more with larger nozzle exit boundary layer swirl angles.

A series of axial velocity contour maps at the center plane as viewed from the jet's small dimension for a half cycle of the free jet evolving motion are shown in Figs. 6 (a)~6(e). The frames have 45° phase difference (time step interval of about 3.2×10^{-5} second) The figure shows clearly both "*flapping*" and "*pumping*" oscillations. From the computation, the "*flapping*" oscillations have a frequency of 3,900Hz, and the "*pumping*" frequency is twice as high as the "*flapping*" frequency. The low velocity field is pushing up the whole jet as time elapses, which causes the jet-tilting phenomenon.

In Figs. 7(a)~7(e), a series of axial velocity contour maps taken at the center plane viewed from the jet's large dimension are presented with frames at 45° phase intervals. The figure shows that the jet spreads out as soon as the jet comes

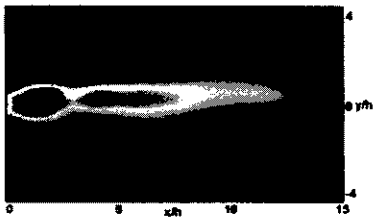
(a)

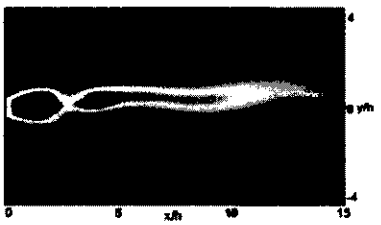
(b)

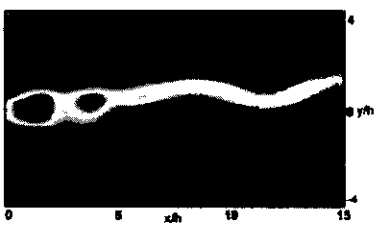
(c)

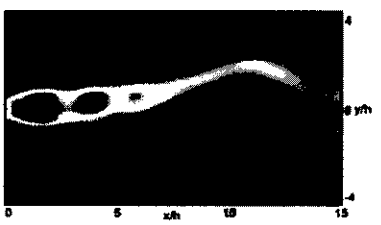
(d)


(e)

Fig. 6 The half cycle of "*flapping*" and full cycle of "*pumping*" oscillations at the center plane in axial velocity contours from jet's small dimension. Phase difference from frame to frame is 45°: $M_j=1.526$

out of the nozzle exit. Consequently the nozzle exit boundary layer swirl angle affects the jet spreading characteristics. Also, because of the

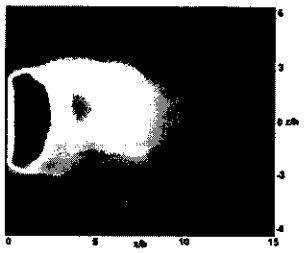
(a)

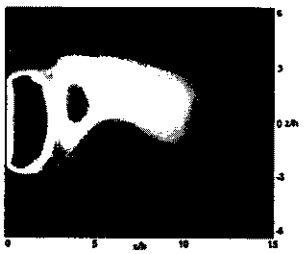
(b)

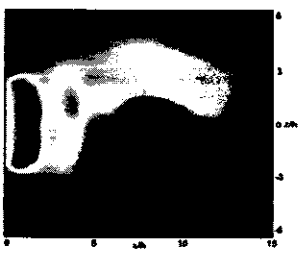
(c)

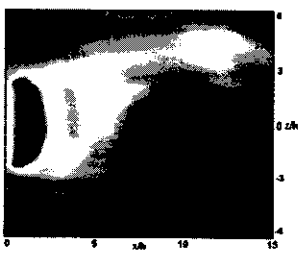
(d)

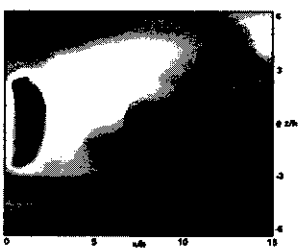
(e)

Fig. 7 The half cycle of "*spanwise*" oscillations at the center plane in axial velocity contours from jet's large dimension. Phase difference from frame to frame is 45°: $M_j=1.526$

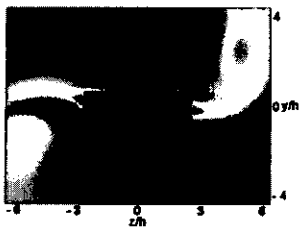

(a)

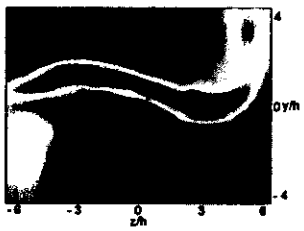

(b)

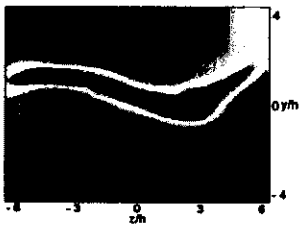

(c)

Fig. 8 Cross-sectional axial velocity contours at jet downstream locations (Swirl angle=45°, M_j=1.526): (a) x/h=0.1, (b) x/h=7.5, (c) x/h=11.5

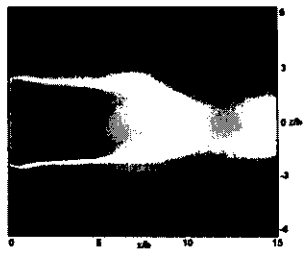

(a)

(b)

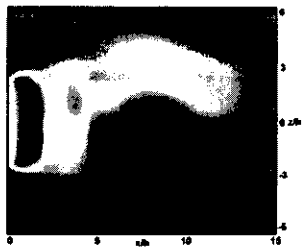

(c)

Fig. 9 Comparison of nozzle exit boundary layer swirl angle effects on axial velocity maps from jet's large dimension: (a) 0° swirl (Han and Taghavi, 1998), (b) 30° swirl (Han and Taghavi, 1999), (c) 45° swirl: M_j=1.526

strong counter-clockwise swirl motion in the nozzle exit boundary layer, the whole jet tilts right. The "*spanwise*" oscillations are also observed at the same frequency as the "*flapping*" oscillations of jet's small dimension. Thus, the jet-tilting, "*flapping*," "*spanwise*," and "*pumping*" oscillations show that the jet is spreading out three-dimensionally. In addition, from Figs. 6 and 7, two shock cells and one relatively weak shock cell are observed at the centerline of the jet as explained previously with Fig. 4.

Cross-sectional axial velocity contours at three downstream locations are plotted in Fig. 8. The contour data in Fig. 8 are at the $\pi/2$-phase of "*flapping*" oscillations. In Fig. 8(a), we can see another high secondary velocity regions in the upper right and lower left corners just after nozzle exit. Those high velocity regions outside the nozzle exit develop because of the high swirl strength. As shown in Figs. 8(b) and 8(c), the high secondary velocity regions spread out as the jet flows downstream. Thus, the high secondary velocity regions enhance jet mixing. The figure, also shows that the jet cross-sectional area grows with axial distance as explained with Figs. 6 and 7.

The axial velocity maps at the center plane as viewed from the jet's large and small dimensions for the cases of 0°, 30°, and 45° nozzle exit boundary layer swirls are illustrated in Figs. 9 and 10, respectively (Han and Taghavi, 1998; Han

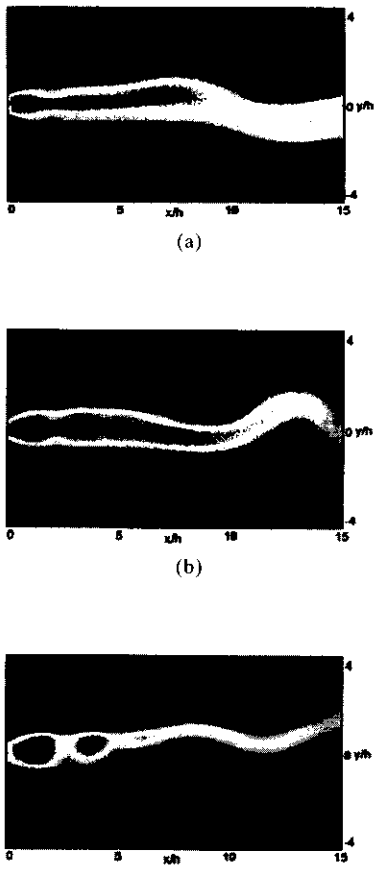

Fig. 10 Comparison of nozzle exit boundary layer swirl angle effects on axial velocity maps from jet's small dimension: (a) 0° swirl (Han and Taghavi, 1998), (b) 30° swirl (Han and Taghavi, 1999), (c) 45° swirl: $M_j=1.526$

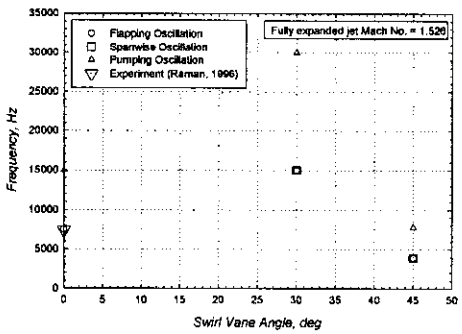

Fig. 11 Frequencies of instability modes in the underexpanded supersonic rectangular jet with nozzle exit boundary layer swirl. 0° and 30° cases are from References (Han and Taghavi, 1998: 1999)

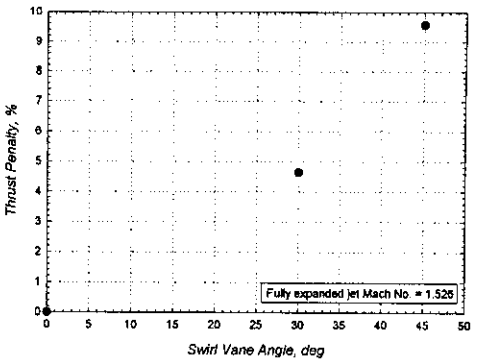

Fig. 12 Thrust penalty due to the addition of boundary layer swirl at nozzle exit. 0° and 30° cases are from References (Han and Taghavi, 1998: 1999)

and Taghavi, 1999). Figures 9 and 10 are selected at phases, which show the instability oscillations clearly for the comparison purpose. Figure 9 shows that the width of jet area at the center plane of jet's large dimension becomes wider as the nozzle exit boundary layer swirl angle increases. Also, the "*spanwise*" oscillations start earlier as the nozzle exit boundary layer swirl angle increases. In addition, Fig. 10 shows that the height of jet area becomes narrower as the nozzle exit boundary layer swirl angle increases. Also, the "*flapping*" oscillations start earlier as the nozzle exit boundary layer swirl angle becomes larger. From Figs. 9 and 10, it is clear that the shock cell area becomes wider as the nozzle exit boundary layer swirl angle increases.

In addition, all of the frequencies of instability modes in the cases of 0°, 30°, and 45° nozzle exit boundary layer swirl cases are shown in Fig. 11. The 30° swirl case shows the highest frequency level. The mixing characteristics of under-expanded supersonic rectangular jet are affected by the combined effects of the jet area and the frequencies of jet instability modes. Also, the instability mode type can be another factor on determining mixing characteristics.

Thus, the boundary layer swirl at the nozzle exit positively affects the mixing behavior of underexpanded supersonic rectangular jet. However, the induction of swirl at the nozzle exit boundary layer reduces thrust produced by the

jet. Thrust penalty is a by-product in the process of enhancing jet mixing. Figure 12 shows the change of thrust penalty vs. swirl angle. The thrust penalty for a 45° swirl case is 10%, which is acceptable in terms of mixing enhancement.

Therefore, the new results and previous results reported (Han and Taghavi, 1998; 1999) show that the nozzle exit boundary layer swirl angle influences "*flapping*," "*spanwise*," and "*pumping*" oscillations and the jet spreading characteristics of jets. Thus, the mixing characteristics of an underexpanded supersonic jet emerging from a plane rectangular nozzle are affected.

4. Conclusion

A three-dimensional unsteady compressible Reynolds-Averaged Navier-Stokes solver with Baldwin-Lomax and Chien's k-ε two-equation turbulence models was successfully used as a computational tool to study the instabilities of underexpanded supersonic jets emerging from plane rectangular nozzles with nozzle exit boundary layer swirl. The aspect ratio of the plane rectangular nozzle used in this study was 5.0, and the fully-expanded jet Mach number was 1.526. A 45° nozzle exit boundary layer swirl ($S=1.0$) was applied at the nozzle exit. The three-dimensional instability characteristics of an underexpanded supersonic rectangular jet (e.g. "*flapping*," "*spanwise*," and "*pumping*" oscillations) were simulated.

From the jet's small dimension views, "*flapping*" oscillations at a frequency of 3,900Hz were observed. Also, "*spanwise*" oscillations were found in the jet's large dimension at the same frequency as the "*flapping*" oscillations. "*Pumping*" oscillations were also observed in the jet's small dimension. The "*pumping*" frequency was twice as high as the "*flapping*" or "*spanwise*" frequency. Also, the thrust penalty due to the addition of 45° nozzle exit boundary layer swirl at the nozzle exit was 10%.

Therefore, the induction of nozzle exit boundary layer swirl is an effective passive excitation technique for enhancing mixing in underexpanded supersonic rectangular jets. However, the strength of nozzle exit boundary layer swirl should be chosen carefully within the acceptable range in terms of thrust penalty.

References

Dash, S. M., Sinha, N., York, B. J. and Lee, R. A., 1990, "Progress in the Development of Advanced Computational Models for the Analysis of Generalized Supersonic Jet Flowfields," *AIAA Paper* 90-3915.

Frank, J. E., 1994, "Experimental Investigation of the Effect of Swirl on Mixing Enhancement of Supersonic Rectangular Jets," M. S. Thesis, The University of Kansas, Lawrence, Kansas.

Gupta, A. K., Lilley, D. G. and Syred, N., 1984, *Swirl Flows*, Abacus Press, England.

Han, S. and Taghavi, R., 1998, "Supersonic Underexpanded Rectangular Jet Oscillations: A Computational Study," *ICAS-98-2.10.5, Proceedings of the 21st ICAS Congress*.

Han, S. and Taghavi, R., 1999, "Effects of Boundary Layer Swirl on Supersonic Underexpanded Rectangular Jet Oscillations," *AIAA Paper* 99-0900.

Jameson, A., Schmidt, W. and Turkel, E., 1981, "Numerical Solutions of the Euler Equations by Finite Volume Methods Using Runge-Kutta Time-Stepping Schemes," *AIAA Paper* 81-1259.

Kim, C. M., Krejsa, E. A. and Khavaran, A., 1994, "Significance of Shock Structure on Supersonic Jet Mixing Noise of Axisymmetric Nozzles," *AIAA Journal*, Vol. 32, No. 9, pp. 1920~1923.

Kim, K. H., Kim, B. W. and Kim, S. W., 2000, "Turbulent Flow Field Structure of Initially Asymmetric Jets," *KSME International Journal*, Vol. 14, No. 12, pp. 1386~1395.

Kim, J. H. and Lee, S. B., 2000, "Supersonic Jet Noise Control via Trailing Edge Modifications," *Proceedings of the First National Congress on Fluids Engineering (KSME)*, pp. 239~242.

Raman, G., 1996, "Cessation of Screech in Underexpanded Jets," *AIAA Paper* 96-1719.

Raman, G. and Taghavi, R., 1998, "Coupling of Twin Rectangular Supersonic Jets," *Journal of*

Fluid Mechanics, Vol. 354, pp. 123~146.

Steger, J. L., 1978, "Implicit Finite-Difference Simulation of Flow about Arbitrary Two-Dimensional Geometries," *AIAA Journal*, Vol. 16, No. 7, pp. 679~686.

Suda, H., Manning, T. A. and Kaji, S., 1993, "Transition of Oscillation Modes of Rectangular Supersonic Jet in Screech," *AIAA Paper* 93-4323.

Yu, Y. K., Chen, R. H. and Chew, L., 1998, "Screech Tone Noise and Mode Switching in Supersonic Swirling Jets," *AIAA Journal*, Vol. 36, No. 11, pp. 1968~1974.